REPORT DOCUMENTATION PAGE		READ INSTRUCTIONS BEFORE COMPLETING FORM
1. REPORT NUMBER NRL Memorandum Report 4387	2. GOVT ACCESSION NO. AD-A092 471	3. RECIPIENT'S CATALOG NUMBER
4. TITLE (and Subtitle) NRL LIGHT ION BEAM RESEARCH FOR INERTIAL CONFINEMENT FUSION		5. TYPE OF REPORT & PERIOD COVERED Interim report on a continuing NRL problem.
		6. PERFORMING ORG. REPORT NUMBER
7. AUTHOR(s) G. Cooperstein, S.A. Goldstein, D. Mosher, R.J. Barker, J.R. Boller, D.G. Colombant, A. Drobot, R.A. Meger*, W.F. Oliphant, P.F. Ottinger*, F.L. Sandel*, S.J. Stephanakis, and F.C. Young		8. CONTRACT OR GRANT NUMBER(s)
9. PERFORMING ORGANIZATION NAME AND ADDRESS Naval Research Laboratory Washington, D.C. 20375		10. PROGRAM ELEMENT, PROJECT, TASK AREA & WORK UNIT NUMBERS DOE-DE-AI08-79DP40092 67-0875-0-0 & 67-0879-0-0
11. CONTROLLING OFFICE NAME AND ADDRESS Department of Energy Defense Nuclear Agency Washington, D.C. 20545 Washington, D.C. 20350		12. REPORT DATE November 20, 1980
		13. NUMBER OF PAGES 39
14. MONITORING AGENCY NAME & ADDRESS(if different from Controlling Office)		15. SECURITY CLASS. (of this report) UNCLASSIFIED
		15a. DECLASSIFICATION/DOWNGRADING SCHEDULE

16. DISTRIBUTION STATEMENT (of this Report)

Approved for public release; distribution unlimited.

17. DISTRIBUTION STATEMENT (of the abstract entered in Block 20, if different from Report)

19. KEY WORDS (Continue on reverse side if necessary and identify by block number)

Inertial confinement fusion
Intense light ion beams
Ion beam focusing
Ion beam transport
Charged particle beam fusion

20. ABSTRACT (Continue on reverse side if necessary and identify by block number)

There is presently great interest in using light ion beams to drive thermonuclear pellets. Terrawatt-level ion beams have been efficiently produced using conventional pulsed power generators at Sandia Laboratory with magnetically-insulated ion diodes and at the Naval Research Laboratory with pinch-reflex ion diodes. Both laboratories have recently focused ion beams to pellet dimensions. This paper reviews recent advances made at NRL in the area of ion production with pinch-reflex diodes, and in the areas of beam focusing and transport. In addition, modular generator and beam requirements for pellet ignition systems are reviewed and compared with the latest experimental results. These results include the following: (1) production of > 100 100 kJ proton and deuteron beams with peak ion powers approaching 2 TW on the PITHON generator in collaboration with Physics International

(Continues)

DD FORM 1473 EDITION OF 1 NOV 65 IS OBSOLETE
1 JAN 73
S/N 0102-LF-014-6601

i

18. Supplementary Notes (Continued)

This paper was presented at the Fifth Workshop on "Laser Interaction and Related Plasma Phenomena," held at the Laboratory for Laser Energetics, Rochester, NY, November 5-9, 1979.

20. Abstract (Continued)

Co., (2) focusing of 0.5 TW deuteron beams produced on the NRL Gamble II generator to current densities of about 300 kA/cm^2, and (3) efficient transport of 100 kA level ion beams over 1 meter distances using Z-discharge plasma channels.

ii

CONTENTS

iii

NRL LIGHT ION BEAM RESEARCH
FOR INERTIAL CONFINEMENT FUSION

1. INTRODUCTION

The use of light ion beams (protons, deuterons, etc.) for inertial confinement fusion has been seriously pursued following the theoretical prediction[1-3] and the experimental documentation[4], that small-area diodes ($\sim$ 100 cm^2) can be used to generate ion beams efficiently at the megavolt-megampere level. Soon after this, results of ballistic beam focusing experiments were presented[5] and a technique for transporting ions in a plasma Z-discharge was introduced[6]. Recently, terrawatt-level ion beams with focused ion current densities in excess of 100 kA/cm^2 have been produced using water-dielectric transmission-line generators at Sandia Laboratories (SANDIA) with magnetically-insulated ion diodes[7] and at the Naval Research Laboratory (NRL) with pinch-reflex ion diodes[8].

Target designs for light ion beams[9] call for delivery of about 2 MJ to an $\sim$ 1 cm diameter pellet in an $\sim$ 10 ns time scale in order to achieve high-gain thermonuclear ignition. Present pulsed power technology provides up to 10 TW single generator modules from which up to 300 kJ of ions can be extracted in 50-100 ns. Thus, a large number of modules and the means to transport energy from these modules onto the pellet are needed. Additionally, compression of the pulse to the pellet-implosion time-scale is required.

Two different approaches addressing these problem areas have emerged. An approach researched by SANDIA[10] involves pulsed-power techniques for shortening the accelerating-voltage pulse, and self-magnetically insulated flow of electromagnetic energy in vacuum transmission lines which terminate in small ion diodes close to the pellet. Packing of transmission lines near the target, coupling of diodes to the lines, and ion-beam focusability will be investigated with the 36 short pulse, 1 TW PBFA I modules now in construction at SANDIA. For pellet ignition, this approach will require on the order of 100 modules.

A second approach, researched by NRL, involves the extraction and focusing of beams from self-insulated pinch-reflex ion diodes, coupled with transport of these focused beams in $\sim$ 1 cm diameter Z-discharge transport channels. Pulse compression during transport to the pellet-implosion time-scale is achieved by increasing the accelerating voltage with time. These techniques are appropriate for modules operating up to the 10 TW level with a 50-100 ns pulse duration. The number of modules required for this approach is on the order of 10.

In the present report, major results of a combined experimental and theoretical study of the second approach are reviewed with concentration on recent advances made at NRL in the area of ion production using pinch-reflex diodes, and in the areas of beam focusing and transport.
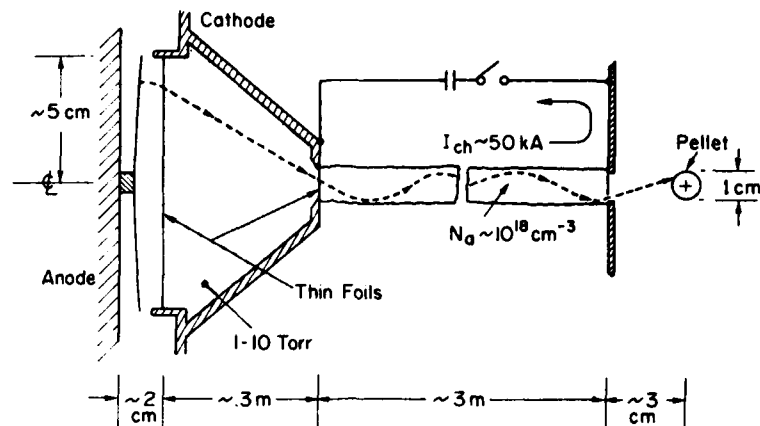
Fig. 1.   Conceptual schematic of NRL Light-Ion Inertial Confinement
Fusion Approach.

A conceptual schematic of the NRL approach is shown in Fig. 1.
The diode and transport system together with the pulsed power genera-
tor (not shown) is one module of a multi-module pellet-ignition
system. A pinch-reflex ion diode ($\sim$ 10 cm in diameter) produces the
ions and properly aims them towards the transport system entrance
aperture. The ion beam then free streams in a gas-filled chamber
towards an $\sim$ 1 cm diameter focus. The gas in the drift region allows
the ion beam to be highly charge- and current-neutralized. Inside
the channel, the ions are confined radially by the azimuthal magnetic
field produced by the discharge of an external capacitor bank. The
$\sim$ 50 kA current in the channel is sufficient to provide radial con-
finement for ions entering the channel with transverse velocities
below about 15% of their axial velocity. The plasma density in the
channel must be sufficiently high to provide inertial resistance to
channel expansion forces during beam transit and sufficiently low
o prevent excessive energy loss of the beam during transport. Beam
power multiplication of about a factor-of-five is achieved during
transport to the pellet by ramping the accelerator voltage in time.
Beams emerging from the channel propagate the last few centimeters
to the pellet with low divergence because of the small transverse
velocity. Several ion beams can then be overlapped onto the pellet.

The second section of this paper discusses ion production in
pinch-reflex ion diodes including recent experiments[11] in collabo-
ration with Physics International Co. on the PITHON generator. In
these experiments, greater than 100 kJ of protons and deuterons were
produced with peak ion powers approaching 2 TW. In Sec. 3, the
self-focusing of ion beams with planar diode geometries is reviewed

and ion focusing experiments with curved geometries are reviewed in Sec. 4. In these experiments, 0.5 TW deuteron beams produced on the NRL Gamble II generator were focused to current densities of about 300 kA/cm^2. In Sec. 5, the numerical simulation of pinch-reflex ion diodes is discussed. Theoretical work on ion orbits in the transport channel is reviewed in Sec. 6, and in Sec. 7 results of recent transport experiments are discussed. In these experiments, high current ion beams have been efficiently transported 1 meter distances using Z-discharge plasma channels. The MHD response of the channel induced by beam passage is then considered in Sec. 8. In Sec. 9, bunching of ion beams in transport channels is briefly discussed. Finally, the results of this research are used to determine a range of system parameters which are appropriate for driving high-gain pellets with proton or deuteron beams.

2.   ION PRODUCTION

Self-pinched electron flow and laminar ion flow in a large-aspect-ratio electron-beam diode are conceptually illustrated in Fig. 2. After an initial phase leading to self-pinched flow[12], the electrons primarily originate from the edge of the cathode and flow under the dominant influence of the self-magnetic fields towards the diode axis ending up in a tight pinch at the center of the anode plane. The ions, which are primarily protons originating from the desorbed gases making up the anode plasma, are only slightly bent
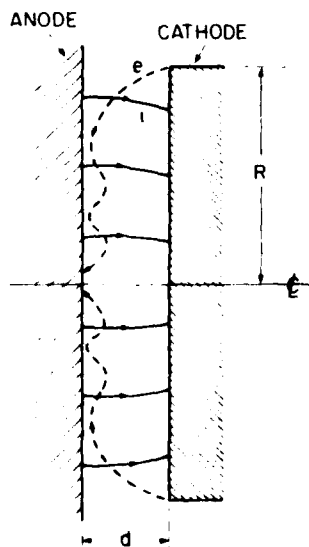

Fig. 2.   Conceptual schematic of electron and ion flow in large-aspect-ratio (R >> d) vacuum diode.

by the diode's self-magnetic fields due to their heavier mass. Thus ions flow in almost straight lines toward the cathode as they accelerate up to the diode voltage. The enhanced ion currents come about because of the additional electron space charge in the diode caused by the large electron path length (R) relative to the ion path length (d). For the simple diode configuration shown in Fig. 2 analytical theory predicts[1] and numerical simulation confirms[13] an ion to electron current ratio of

$$\frac{I_i}{I_e} > \frac{R}{d}\left(\frac{eV}{2m_i c^2}\right)^{\frac{1}{2}}$$

where R is the diode radius, d is the anode-cathode gap spacing, V is the diode voltage and m_i is the ion mass.

Early experimental results[14] with $R \simeq 6$ cm and $d \simeq 0.4$ cm giving $(I_i/I_e) \sim 1/2$ were in excellent agreement with this theory. These demonstrated 0.8 MeV proton currents of up to 200 kA. Using spherical section electrode structures, focused deuteron current densities of up to 70 kA/cm^2 were obtained[15]. These early results were obtained at 0.5 TW with the Gamble II generator operated for the first time in positive polarity. In positive-polarity operation, the cathode is mounted on the door of the generator so that ions accelerated through the diode potential can be injected into a drift tube region through a thin cathode transmission foil.

In the most recent positive polarity experiments[8] on upgraded[16] Gamble II at 1.5 TW, $\sim 60\%$ conversion efficiency from generator power to ion power was achieved using the refined diode design illustrated in Fig. 3. A thin CH_2 foil stretched across a dielectric ring is electrically connected to the positive electrode by a 1 cm-diameter rod on the diode axis. Plasma formation due to surface flashover causes the plastic foil to become a conductor early in the pulse and provides a source of ions. This geometry enhances ion emission by increasing the electron path length (and therefore lifetime) relative to that of ions by forcing the electrons to reflex through the thin foil as they pinch in radially. This reflexing is not due to spatial charge building up in the vacuum gap behind the foil because this is quickly neutralized by ions from the anode plasma. Rather, it is due to the azimuthal self-magnetic field caused by the return current flow through the center conductor. Thus, electron reflexing is magnetically induced behind the foil. In front of the foil, the electrons reflex in the self-consistent diode fields. The ions that are produced on the back of the anode foil do not carry diode current because the back plate is at anode potential. Results of the numerical simulation of this diode configuration will be presented in Sec. 5.

Fig. 3. Pinch-reflex diode schematic.

Typical diode electrical characteristics are shown in Fig. 4a for a 6 cm cathode radius, a 0.4 cm anode-cathode gap spacing, and a 0.5 cm vacuum gap behind the 0.01 cm CH_2 anode foil. Ion currents of 500 kA have been measured with 1 MA total diode currents. This corresponds to an average source *ion* current density of 5 kA/cm^2. After passing through a phase associated with establishing the charged-particle flow illustrated in Fig. 3, the diode impedance remains well matched to the 1.5 ohm output impedance of the Gamble II generator. Closure of the anode-cathode gap due to electrode plasma motion usually occurs near the end of the electrical power pulse. The diode impedance can be adjusted by varying the cathode emitting area, the anode-cathode gap spacing, or the applied voltage. The natural voltage ramp which occurs demonstrates that accelerating voltages appropriate for ion bunching during transport to fusion pellets can be achieved with these generators. The net current signal (the current entering the cathode foil) is interpreted as the total ion current flowing in the anode cathode gap. The location of the Rogowski coil used to make this measurement will be illustrated later in Fig. 6. On a few selected shots, the measured net current exceeded 700 kA at 1.3 MV out of 1.1 MA of total diode current. Carbon activation[17] by proton beams indicates that greater than 50% of the net-current signal is due to protons. The interpretation of these results is limited by an unknown correction for deuteron activation. When the anode is coated with CD_2, neutron time-of-flight measurements show that greater than 50% of the net current takes the form of deuterons. Up to 10^{12} neutrons have been measured on Gamble II. This data is consistent with ion

5
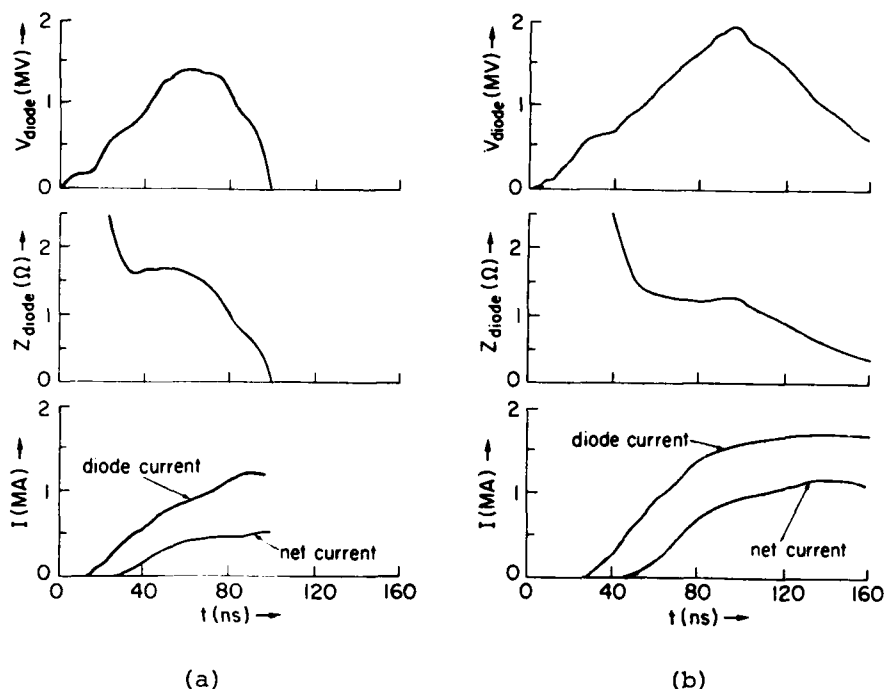
Fig. 4. Diode electrical characteristics for (a) Gamble II and
(b) PITHON.

energies of at most 300 kV lower than the diode voltage of 1.3 MV.
Several mechanisms are being investigated as a source of this loss.

In the most recent ion production experiments[11], a pinch-reflex
ion diode, similar to that used on Gamble II (Fig. 3), was successfully
operated at 3 TW on the Physics International PITHON generator. The
main difference between the geometry used on Gamble II and that used
on PITHON was that PITHON presently only operates in the normal
negative polarity mode. Because the cathode was now at a 2 MV poten-
tial, this required special techniques to be able to both read out
the ion current monitors and to fill the drift region behind the
cathode with gas. Deuteron current measurements were made in the
conventional manner by coating the anode foil with CD_2 and using
both nuclear activation and time-of-flight neutron detectors to
detect the neutrons produced from a (greater than one range thick)
CD_2 target placed behind the cathode.
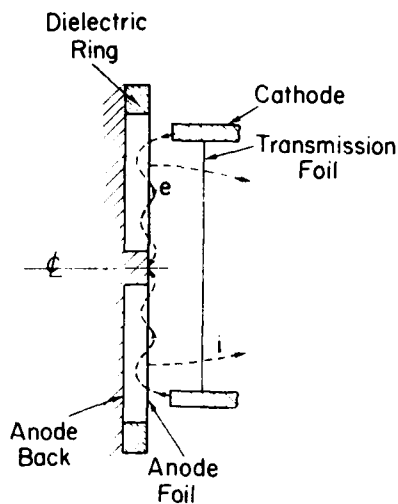
Typical diode electrical characteristics are shown in Fig. 4b
for a 6 cm cathode radius, a 0.3 cm anode-cathode gap spacing, and
a 0.5 cm vacuum gap behind the 0.01 cm CH_2 anode foil. Peak diode
voltages of 2 MV at 1.5 MA diode current were obtained with flat
impedance behavior even though the pulse length was almost twice as
long as that on Gamble II. Ion currents of up to 1 MA were obtained

6

corresponding to peak ion powers approaching 2 TW. Over 100 kJ of
ions were produced out of just over 200 kJ of electrical energy
delivered to the diode. Impedance control and electrical reproduc-
ibility were excellent. When deuterons were produced, the neutron
yield approached 10^{13} from the D-D and D-carbon reactions occurring
in the CD_2 target.

As will be discussed in the last section, the voltage and ion
currents produced on PITHON are in the range for a single module of
a multi-module pellet ignition system. The long impedance lifetimes
and high reproducibility associated with the $\sim$ 1 cm gap between the
anode and cathode transmission foil indicates that programmed-voltage
waveforms for beam bunching during transport can be employed. Focus
perturbing effects associated with time varying B_θ fields in the
diode region can be controlled for these $\sim$ 1 cm diode gap by elec-
trode shaping and naturally occurring gap closure as discussed in
the next section.

3.   ION FOCUSING IN PLANAR GEOMETRY

The processes believed to be important in ion focusing are sche-
matically illustrated in Fig. 5. Ions traversing the vacuum gap
are radially accelerated inward by the azimuthal magnetic field of
the diode current flow. Particle-in-cell codes predict that the
predominant electron flow in the diode is close to the anode surface
where most of the potential drop across the diode takes place. Thus,
the electron current contributes to the angular deflection of ions
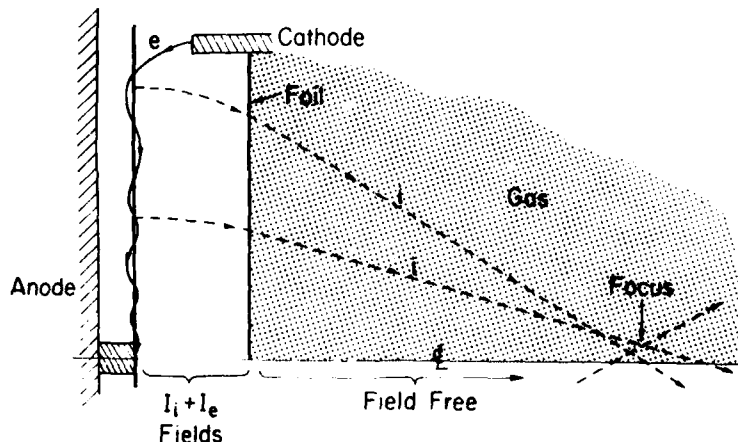only for a small fraction of the vacuum space. The ions are radially

Fig. 5. Light ion focusing schematic.

7

accelerated primarily by their own current. If the ion current density were approximately uniform over the anode surface, then the resulting linear $B_\theta(r)$ would cause the ions to be pointed towards an approximately-common focus as they enter the cathode transmission foil. Scattering during passage through the 1.8 μm polycarbonate (KIMFOL) foil is about 20 mrad for 1 MeV protons. Beam induced breakdown of the low pressure gas filling the drift region to the right of the cathode foil allows beam current neutralization. The magnetic field acting on the ions is reduced by a factor of 50 by this neutralization. The ions have therefore nearly straight-line trajectories in this region and free stream towards the focus.

One major limitation to tight focusing is asymmetry in power and charged particle flow in the diode. This can be overcome by careful experimental design which results in well-centered electron pinches and centered symmetric ion focal spots. Another major limitation is the actual radial distribution of ion current which may direct ions emitted at different radii to different foci. In principle, for a given diode voltage and current, the shapes of the anode and cathode surfaces can be adjusted to correct for focus-perturbing effects of non-uniform ion current distributions. For instance, the launch angle can be changed by curving the anode surface. The radial deflection due to diode magnetic fields can also be changed by varying the axial position of the cathode foil as a function of radius. The anode-foil thickness can also be varied as a function of radius to vary the degree of electron reflexing and thus control the emitted ion current profile. A final major limitation to tight focusing is the time variation in the focusing magnetic fields which cause a change in focus location with time. This effect can be partially offset by the natural reduction of the anode-cathode (AK) gap due to electrode plasma motion. Thus, as the diode current increases, the increasing radial acceleration of the ions can be offset by the reduction of AK gap with time. In principle, both the initial AK gap spacing and the cathode foil material could be chosen to minimize this time variation effect.

Long focal lengths (i.e. large f-numbers) are achieved by magnetic self-focusing acting alone in a flat-anode geometry. This configuration is employed to inject ions into transport channels since larger-angle injection requires excessive transport-channel currents. Spherically-curved anodes in conjunction with self-magnetic forces are used to obtain shorter focal-lengths appropriate for target studies with the highest-focused current densities.

Three sets of focusing experiments in planar geometry were performed on Gamble II with electrical characteristics similar to those of Fig. 4a.
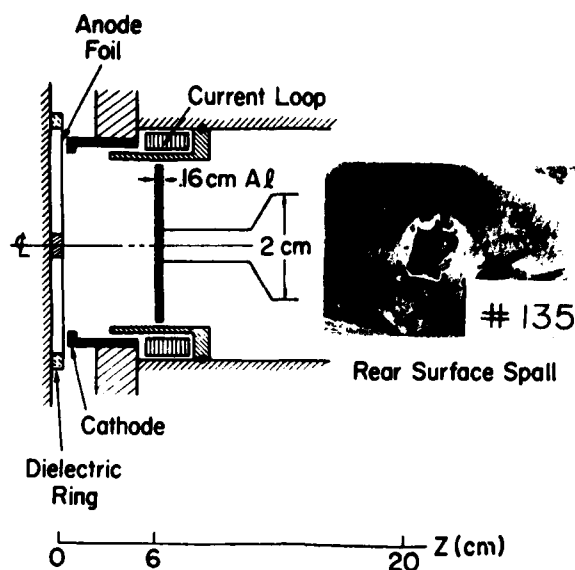
Fig. 6. Self-focusing in planar geometry with no cathode foil.

The first self-focusing experiments were performed with the planar diode geometry illustrated in Fig. 6 where a 0.01 cm thick CH_2 anode foil stretched across a dielectric ring was used with a 12 cm diameter hollow cathode without a cathode transmission foil. The ion beam was observed to self-focus 6 cm from the anode as indicated by the 1 cm^2 rear surface spall produced on a 0.16 cm thick aluminum witness plate. No spall was observed when the witness plate was placed a few centimeters to either side of this position. The focus location was in agreement with self-consistent analytical and numerical calculations for the self-focusing of a 500 kA, 1.3 MV proton beam. These calculations consist of solving ion orbit equations in the diode electromagnetic fields (determined from current and voltage measurements) and in the focusing/drift region magnetic fields (determined from net current measurements).

In the second set of self-focusing experiments, the 1.8 µm thick cathode foil was placed at 4 mm from the cathode face as shown in Fig. 7, and the drift tube was evacuated. A Rogowski coil in the evacuated drift tube measured a net current of about ½ the total ion current. The ion self-focus, as determined from the rear surface spall of the witness plate, moved from 6 cm to about 12 cm from the anode plane, again consistent with the predicted location for this reduced net current in the drift section. The origin and nature of this net current has been discussed[18].

9
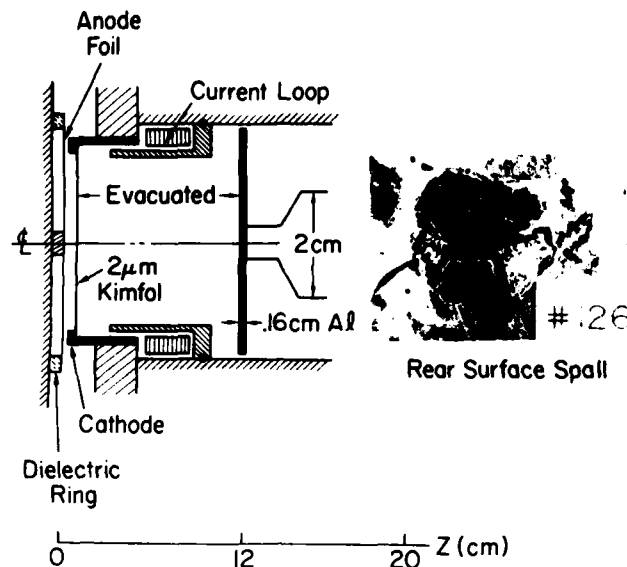
Fig. 7. Self-focusing in planar geometry with cathode foil and
         evacuated drift tube.

The final self-focusing experiments were performed with the
cathode foil 2.8 cm from the anode and with the drift tube region
behind the foil filled with 2 Torr of air. The large separation
between the anode and the cathode foil insured that negligible elec-
tron current flowed from the cathode foil to the anode. This experi-
ment is illustrated in Fig. 8. The cathode foil was bowed by the
air pressure in the drift tube. The Rogowski coil surrounding the
cathode foil support structure monitored the total current flowing
into the cathode foil. The second Rogowski coil in the drift tube
read less than 2% of the current read by the first for drift
tube pressures between 0.2 to 3 Torr. With gas in the drift
section, an aluminum witness plate placed at the 20 cm predicted
focus location showed a 3 cm diameter rear surface spall. Computer
analysis predicting ion orbits indicates that the 2-3 cm diameter
focus spot size is consistent with axial motion of the best-focus
location due to the time variation of diode current and voltage.
That is, although the current and voltage values may be appropriate
for tight focusing at peak power, the beam is under-focused early
and over-focused late in time. No spall occurred a few centimeters
to either side of this position and moving the cathode foil moved
the focus location as predicted. It is important to note that
damage patterns associated with focusing in the neutralizing gas
backgrounds of this last set of experiments were typically well
centered and symmetrical, whereas, focal spots obtained in vacuum
display azimuthal irregulatiries and beam filamentation. Aluminum

10
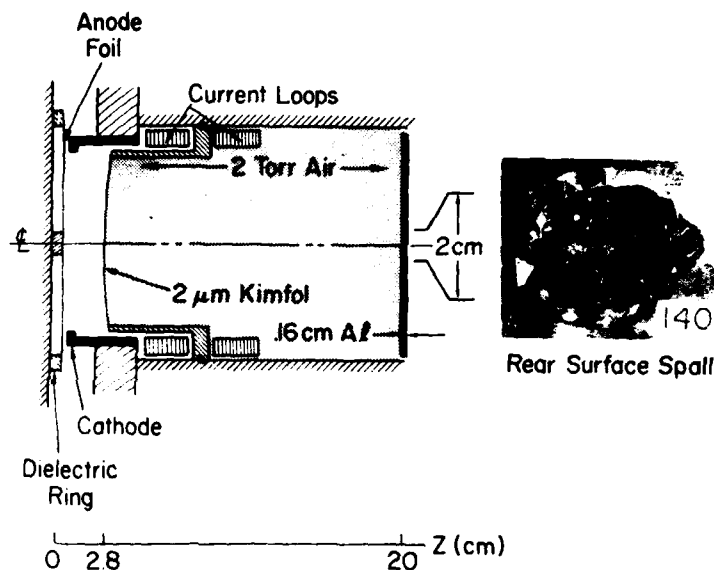
Fig. 8. Self-focusing in planar geometry with cathode foil and
        gas in drift tube.

K_α x-ray pinhole photographs[7] showed a peak current density of about
50 kA/cm^2.

4. ION FOCUSING IN CURVED GEOMETRY

In order to achieve high ion current densities for beam target
experiments, a 0.025 cm thick spherical-section plastic anode foil
with a 12.7 cm radius of curvature was used. As shown in Fig. 9,
the same cathode geometry previously shown was employed except for
the closer proximity of the thin cathode transmission foil to the
cathode surface. In this short-focal-length geometry, the ion
launching angle dominates over the magnetic deflection in the diode.
Focal spot broadening due to radial and temporal field effects is
thus minimized. Aluminum witness plates placed at the best focus
location exhibit smaller area spall patterns (1-1.5 cm diameter)
than in flat geometry with gas. When the anode was coated with
CD_2, the observed focus was close to the geometric focus because of
the small magnetic deflection of deuterons. By using small CD_2
targets and measuring neutrons from D-D and D-carbon reactions with
activation counters and time-of-flight detectors, peak deuteron
current densities of about 300 kA/cm^2 over 0.5-1 cm^2 were inferred.
Typical neutron yields were a fraction of 10^{12} neutrons.

Important new experimental results for focusing are provided
by a pinhole shadowbox diagnostic shown in Fig. 10. Small ion

11
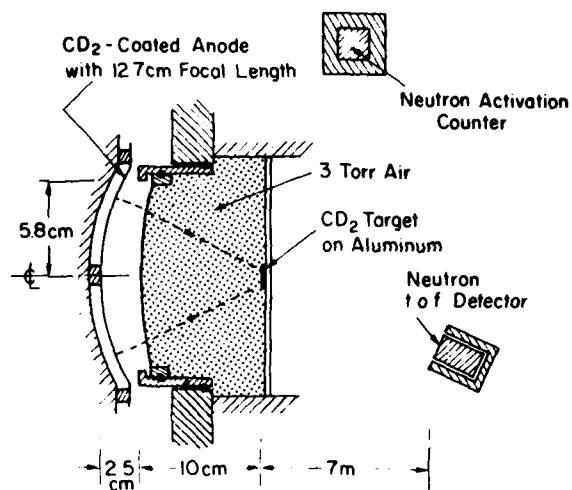
Fig. 9. Geometric focus experiments.
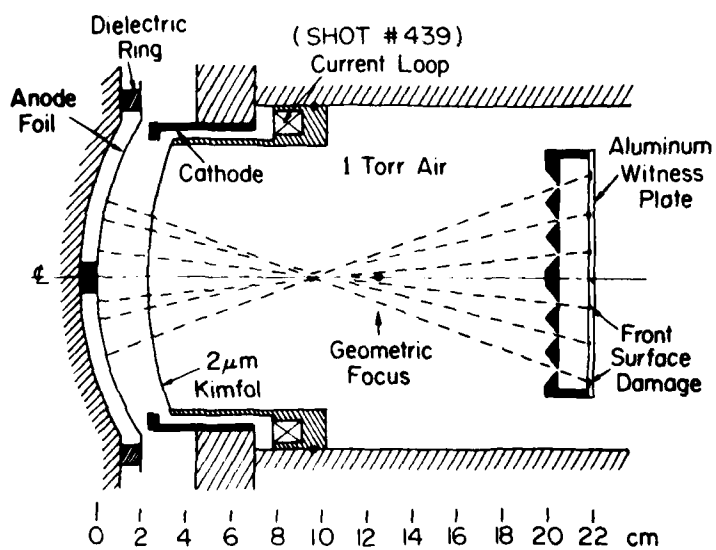
Fig. 10. Ion pinhole shadowbox.

12

beamlets are produced by masking off all of the beam drifting in the neutralizing background except for that portion emerging through 1 mm diameter holes placed along two diameters at right angles. Damage patterns produced on a aluminum witness plate 1 cm behind the pinhole array (shown as solid spots in the figure) allows one to determine ballistic orbits for ions entering pinholes at various radii. When the shadowbox is placed further from the diode than the center of the ion focus, these orbits can be projected from the damage spots back through the pinhole to the focus. These are shown as dashed lines in the figure. In this manner, the best focus location and the radial dependence of ion deflection angle can be determined. Additionally, the radial extent (typically a few millimeters) of each damage pattern reflects the time-variation of deflection angle due to time-varying diode fields. The preliminary Gamble II results with protons demonstrate that radial deflections of damage patterns (shown in Figure 10) are consistent with the measured focus location. Diode deflection angles were found to be roughly proportional to radius. Also, the significantly smaller observed azimuthal extent of damage compared with the radial extent of damage suggests that with proper aspheric anode and cathode shapes, focusing of ion beams to areas very much less than the present 1-3 cm^2 should be possible.

5. NUMERICAL SIMULATION OF PINCH-REFLEX ION DIODES

Numerical simulations of electron and ion flow in pinch-reflex diodes were conducted for the configuration shown in Fig. 11 using the NRL DIODE2D simulation code.[19] The initial equipotential lines are also shown in the figure. The diode dimensions modeled in the simulation had an R/d=20 aspect-ratio where r=6.8 cm was the outer radius of the hollow cathode and d=0.32 cm was the separation of the cathode face from the anode foil. The thickness of the cathode shank was 0.8 cm and the scattering foil was assumed to be 125 μm thick polyethylene. The distance between the reflexing foil and the solid anode was 0.29 cm. This space was assumed to be filled with ions which charge neutralize the reflexing electrons, making it unnecessary to solve for the electrostatic fields in that region. The distance from the reflexing foil back to the ion transmission foil inside the hollow cathode was 0.7 cm. These new simulations were carried out on a finer 64×40 mesh rather than the 32×40 mesh used in previously reported results.[20] The simulations also assumed azimuthal symmetry and were done in (R,Z) geometry with a time step of 0.25 psec.

The time evolution of the electron and ion flow in the diode is shown in Fig. 12 for a simulation done at 1.5 MV. The positions of the electrons and ions are shown in (R,Z) configuration space at four different times. Early in time (step 500), the electrons (one in 10 is plotted on the figure) had transited the diode and

13

0.32cm

CATHODE
SHANK

ANODE
REFLEXING
FOIL

0.8 cm

SOLID
ANODE

α   6.0cm

RETURN
CURRENT
ROD

0.6cm

TRANSMISSION
FOIL

.704cm

.288cm

0.0125cm

Z →
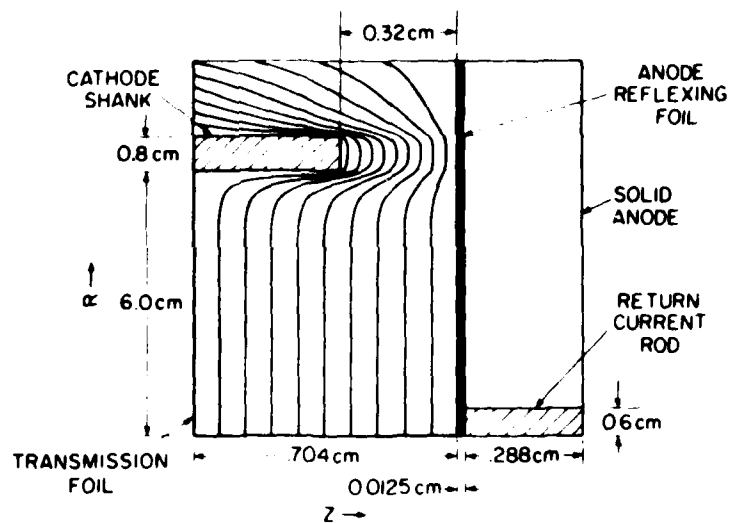
Fig. 11.   Configuration used for pinch-reflex diode simulation
showing equipotential lines due to applied voltage.

TIME
STEP   500   1000   1500   2500

ELECTRON POSITIONS
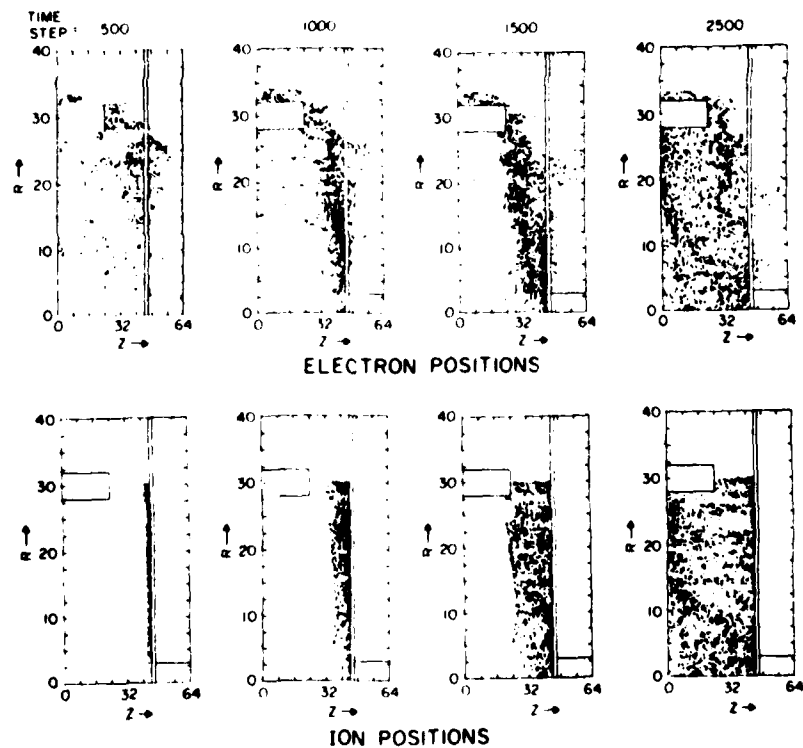
ION POSITIONS

Fig. 12.   Time history of the electron and ion positions in the
diode.

14

reflexed several times through the foil. The ions had not yet
crossed the diode gap and were clumped along the anode foil. By
time step 1000, the electrons had established the pinched flow
along the diode side of the reflexing foil. At step 1500, the
pinched electron flow was well established and the electrons filled
the diode gap. However, electrons did not flow along the foil except
at low radii because of the tendency for electrons to follow ions
at large radii to provide space charge neutralization. At step 2500,
all the ions had now crossed the gap and a quasi-steady state was
established. The flow pattern shown at step 2500 persisted for the
remainder of the run which was taken to step 4000.

In the quasi-steady state the equipotential lines are piled
up near the anode foil so that most of the potential drop occurs
over a distance much less than the 0.32 cm gap between the cathode
face and the anode foil. This justifies the assumption of Sec. 3
that the ion bending between the anode and cathode foil is primarily
due to the self-magnetic field of the ions. The current density
profile of the ions arriving at the cathode transmission foil is
shown in Fig. 13. This current profile, which is the result of
averaging the arriving ion current for 500 time steps, shows a
1/R dependence as predicted by analytic theory[2] for planar diodes.
The simulation for this case assumed that ion emission occurred
along the reflexing foil up to a radius of 6.4 cm. In this case,
the net ion current was 590 kA and the electron current 330 kA.
In order to determine if the average ion current density could be
increased by suppressing ion emission at large radii, a case where
emission was allowed only up to a radius of 3.0 cm was also
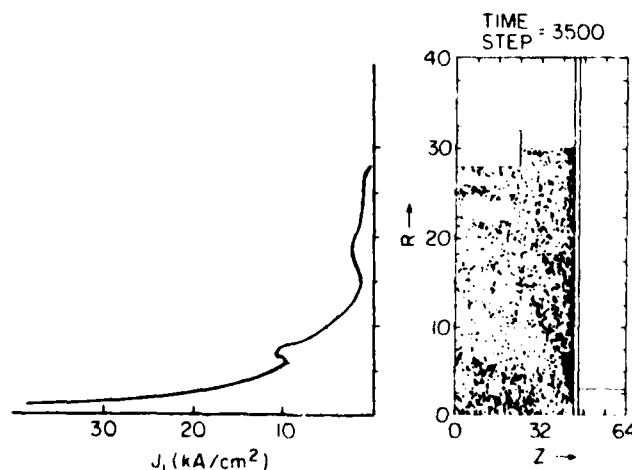
Fig. 13. Ion current density profile at the cathode and ion
positions in the quasi-steady state.

15

simulated. In this case, the total diode current remained close
to 900 kA and the total ion current decreased by about a factor
of 2.

The simulation results are in reasonable agreement with the
NRL experimental data with respect to total ion and electron
currents. The geometry was different enough so that it is difficult
to make a more quantitative statement. The transmission foil is
further removed from the cathode face in the present Gamble II
experiments than in the simulation and this may affect the diode
behavior. Further simulations that are closer to the actual experi-
mental configurations are being conducted so that a more direct
comparison with experiments can be made.

6. ION ORBITS IN Z-DISCHARGE CHANNELS

As shown in Fig. 14, ions enter the discharge channel with a
range of injection angles up to θ_M determined by the anode radius
and distance to the focus. The externally-applied current flowing
through the channel must be sufficient to confine ions with maximum
transverse kinetic energy, that is, ions which enter the channel
with the maximum injection angle at the maximum injection radius,
r_s. The required discharge current can be determined from conser-
vation of ion energy and P_z conical momentum

$$v_r^2 + v_z^2 = v_o^2 \; ; \qquad v_z = v_o \cos\theta + \frac{q}{m} \int_{r_o}^{r} B_\theta(r')dr' \quad ,$$

where $\frac{1}{2}mv_o^2$ is the energy of an ion with charge q, θ is the injection
angle and r_o is the injection radius. In order for the magnetic
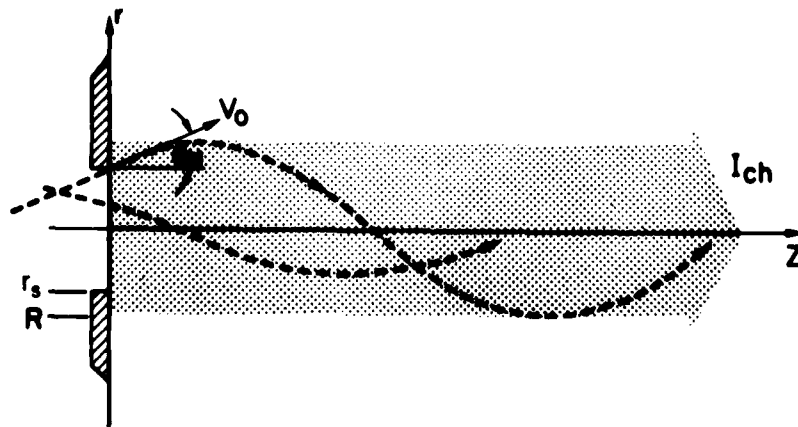
Fig. 14. Ion orbits in a Z-discharge channel.

field to be just sufficient to confine a maximum-transverse-energy ion to the channel radius (R), V_r must vanish when $r = R$ for initial conditions $\theta = \theta_M$ and $r_o = r_s$. Substituting into the previous equation, results in the expression

$$q \int_{r_s}^{R} B_\theta dr = mV_o (1-\cos\theta_M) . \tag{1}$$

Defining an ideal channel as one carrying a uniform discharge current so that $B_\theta \sim r$ when $r \leq R$, Eq. (1) takes the form

$$I_{ch}(A) = \frac{10^{-3}V_o(1-\cos\theta_M)}{1 - (r_s/R)^2} \tag{2}$$

for protons where I_{ch} is in amperes when V_o is in cm/s. This result indicates that megampere discharge currents are required to confine ions injected with large angles. Protons of 5 MeV with $\theta_M = 0.2$ radians require about 120 kA for confinement within the channel when $r_s/R = 2/3$.

Analytical and computational techniques have been used to determine the effects of various forms of nonideal channel behavior on ion confinement and beam bunching.[21] Axial electric fields associated with plasma currents and expansion disrupt confinement and reduce beam power multiplication due to bunching only if large enough to strongly slow the beam during transport. Radially non-uniform net currents develop as the beam passes through the back-ground because of beam-induced MHD expansion of the channel. The effects of the resulting B_θ fields on beam confinement are discussed in Sec. 8. Channels which taper to smaller radius as they approach the pellet were investigated as a means of increasing the beam current density. A WKB-like analysis for the ion motion shows that only a small improvement in current density due to radial beam compression can be achieved before disruption of axial compression by bunching. Both analytic and numerical calculations were performed to determine ion confinement in a channel with a large amplitude $m = 0$ sausage instability. Fig. 15 shows one result of this work. The channel B_θ was modeled as $\sim r$ inside the channel radius $R(z)$, and $\sim 1/r$ outside. With every change in axial location $\Delta z = \lambda$, the value of R changed abruptly and randomly to simulate the non-linear development of the instability. A large number of ion orbits were numerically determined for a range of injection angles up to θ_M and injection radii up to r_s. The figure shows a cross-section of beam ion density at various axial locations along the channel. The case shown corresponds to $r_s = 0.4$ cm, $R = 0.6$ cm, $E_i = 5$ MeV, $\theta_M = 0.2$ radians, $I_{ch} = 120$ kA, $\lambda = 3.8$ cm, $\Delta R_{rms}/\bar{R} = 1$. This high
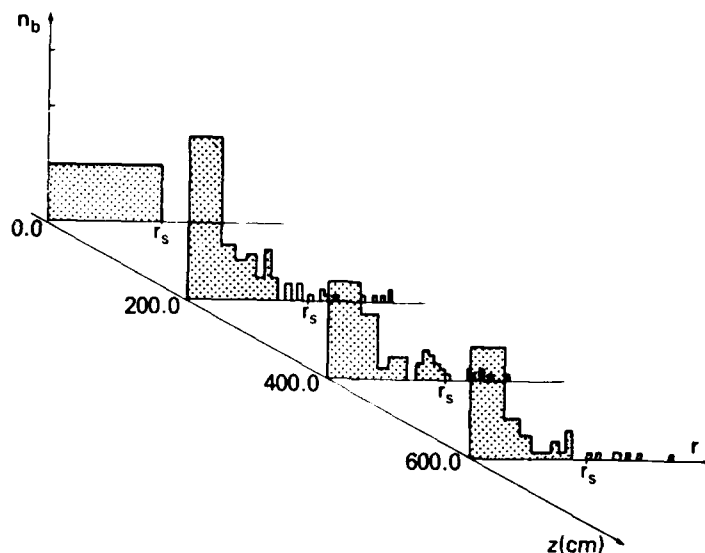
Fig. 15. Beam density profile at various axial locations along
a sausage unstable channel.

degree of fluctuation is required for radial loss of half the beam
ions after transporting 6 m. When ΔR_{rms} is decreased by about a
factor of 2, only about 9% of the beam is lost at 6 m. Good radial
confinement is predicted for all cases in which the axial wave
length of the instability is much smaller than the betatron wave-
length of the ion in the channel. Electrostatic and electromagnetic
microinstabilities driven by the relative streaming between the
beam ions and the channel plasma have been discussed previously.[22]

7. ION TRANSPORT EXPERIMENTS

Figure 16 illustrates the experimental configuration for
transport experiments on Gamble II. The planar, pinch-reflex diode
configuration shown previously in Fig. 8 was used to bring a 0.5 MA,
1.4 MV proton beam to a narrow-angle focus ($\sim$ 50 kA/cm^2) 20-30 cm
downstream from the diode. The transport section consisted of a
copper pipe containing an insulating ceramic liner filled to the
0.2-2 Torr air background pressure of the focusing-drift section.
The inside diameter of the ceramic liner defines the diameter of
the wall-stabilized discharge. A discharge channel diameter of
4.5 cm was employed. The discharge current was provided by a
20 kV, 10 kJ capacitor bank. The current rose to about 50 kA in
15 μs after which time the ion beam was injected into the channel.
This current satisfies Eq. (2) for the injection angles employed
in the experiment. Measurements of transport efficiency were
provided by diagnosis of 6 MeV gamma rays produced by the inter-
action of beam protons with fluorine[23]. Collimated scintillator-

18
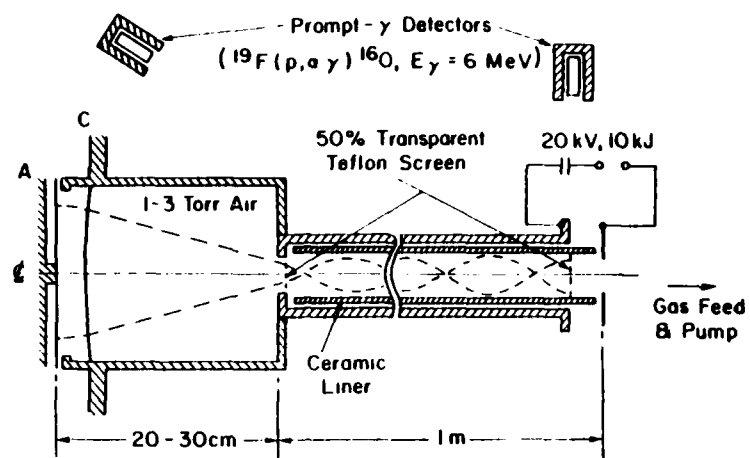
Fig. 16. Ion transport experiment schematic.
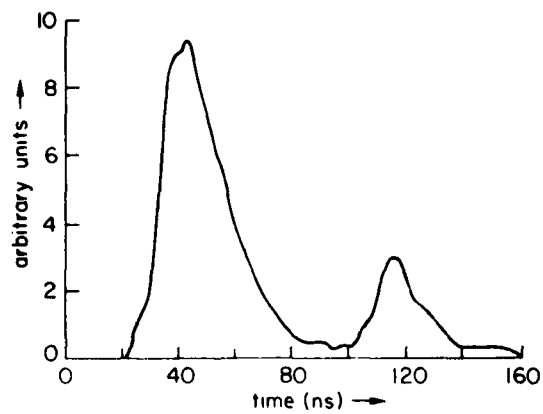
Fig. 17. Prompt-γ signal from two 50% transparent teflon targets placed on meter apart in the channel.

photomultiplier detectors were used to detect the gamma rays produced in 50% transparent teflon screens placed at the entrance and exit apertures of the transport system.

The signal shown in Fig. 17 was obtained with a single detector placed about 4 m from both screens and behind about 0.5 m of concrete. Signals from the two screens are separated by the ion time-of-flight through the 1 m discharge channel. Because the teflon screens are 50% transparent, the second signal must be multiplied by a factor of 2 in order for comparison with the signal from the entrance aperture. Since the gamma-ray production cross-section is a strong function of the proton energy, the transport efficiency could not be immediately inferred from the ratio of signals associated with the two screens. Assuming no ion energy loss during transport, experimental results indicated a lower limit of 50% transport efficiency. If an energy loss of 200 kV is assumed, which is consistent with the relative timing between the prompt-γ signals shown in Fig. 17, then the particle transport efficiency in the channel is about 80%. A more concrete example of the ability to transport ion beams is provided by witness plates at the exit aperture. Aluminum plates 0.16 cm thick exhibited rear surface spalls with widths less than the channel diameter. Null experiments, measurements without channel current, did not show evidence of ion transport.

In more recent transport experiments a smaller 1.6 cm diameter channel was used with a much faster risetime (0.5 μs) capacitor bank than previously employed. Preliminary results indicate that proton beams with current densities of several tens of kA/cm^2 were efficiently transported over 1 m distances. Unlike the large diameter channel transport experiments, shots were taken with the ion beam injected into the channel while the channel plasma was still radially imploding. On these shots, the shapes and relative timing of the input and output prompt-γ signals suggest that the protons may have gained rather than lost energy in the channel. This observation would be consistent with recent theoretical predictions[24] that the transported ion beam could gain energy from the fields associated with a radially imploding Z-pinch plasma. This phenomenon is presently under investigation.

8.   RESPONSE OF THE CHANNEL TO BEAM TRANSIT

As the focused ion beam transits the transport channel, it heats the background plasma by collisional deposition and induces plasma-electron return currents which resistively heat the plasma. Since the electromagnetic fields induced by the beam can vary substantially from those assumed to confine the beam ions, it is important to determine how the self-consistent fields alter beam confinement and energy loss during transport. To answer these

20

questions, a 1-D radial, time-dependent MHD code has been developed[25]. The code solves the usual conservation equations for particle number, momentum and energy. The $\vec{V} \times \vec{B}$ and $\vec{V} \times \vec{E}$ Maxwell's relations, and electron transport equations (using classical coefficients for electrical and thermal conduction) close the set of equations. The beam is specified by its current density in space and time and the particle energy as a function of time. Collisional beam deposition and plasma-electron return-current heating are included as is bremsstrahlung radiation cooling. Development of radial profiles in time for background density, electron and ion temperature, azimuthal magnetic field and radial velocity are shown in Fig. 18 for a 50 kA discharge in deuterium carrying 600 kA of 5 MeV protons in a 50 ns pulse. Since the plasma is initially at rest, no radial velocity profile is shown in Fig. 18a. The initial temperature distribution is thus determined by an equilibrium pressure balance condition. Once the beam enters the channel, the plasma pressure and $\vec{j} \times \vec{B}$ forces acting on the plasma push material out of the channel interior and pile it up against the steep density gradient at the channel edge. The initial magnetic field profile corresponds to uniform current density arising from the long times and the low conductivities associated with channel creation. Once the beam heats the channel (Fig. 18b), the conductivity rises quickly and magnetic field lines become frozen in the plasma. The magnetic field is then convected out of the center of the channel along with the plasma flow.

A primary criterion for maintenance of beam confinement is suggested by Eq. (1) and is given by the integral extended from r_0 to R. If the value of the integral is reduced, ions injected with large r_0 or θ_0 can reach the high density edge of the channel and be lost. For low beam current cases, the plasma channel response to the beam is sufficiently gentle not to disrupt confinement. However, in the high-current cases, ions with larger transverse energy are lost.

The evolution of the confinement integral with time does not depend sensitively on the ion energy. This behavior can be understood qualitatively by examining the plasma equation of motion.

$$\rho \frac{dV_r}{dt} = -\frac{\partial p}{\partial r} - j_z B_\theta \approx j_b B_\theta \tag{3}$$

The final expression on the right hand side of Eq. (3) results from the dominance of the $\vec{j} \times \vec{B}$ term over the pressure term and good beam current neutralization. For a maximum allowed acceleration given by $2R/\tau^2$, where τ is the beam duration, Eq. (3) yields

$$I_b I_{ch} < 300 \, \rho \, R^4/\tau^2 \tag{4}$$

for maintenance of beam confinement. In Eq. (4), the currents are

(a)

(b)
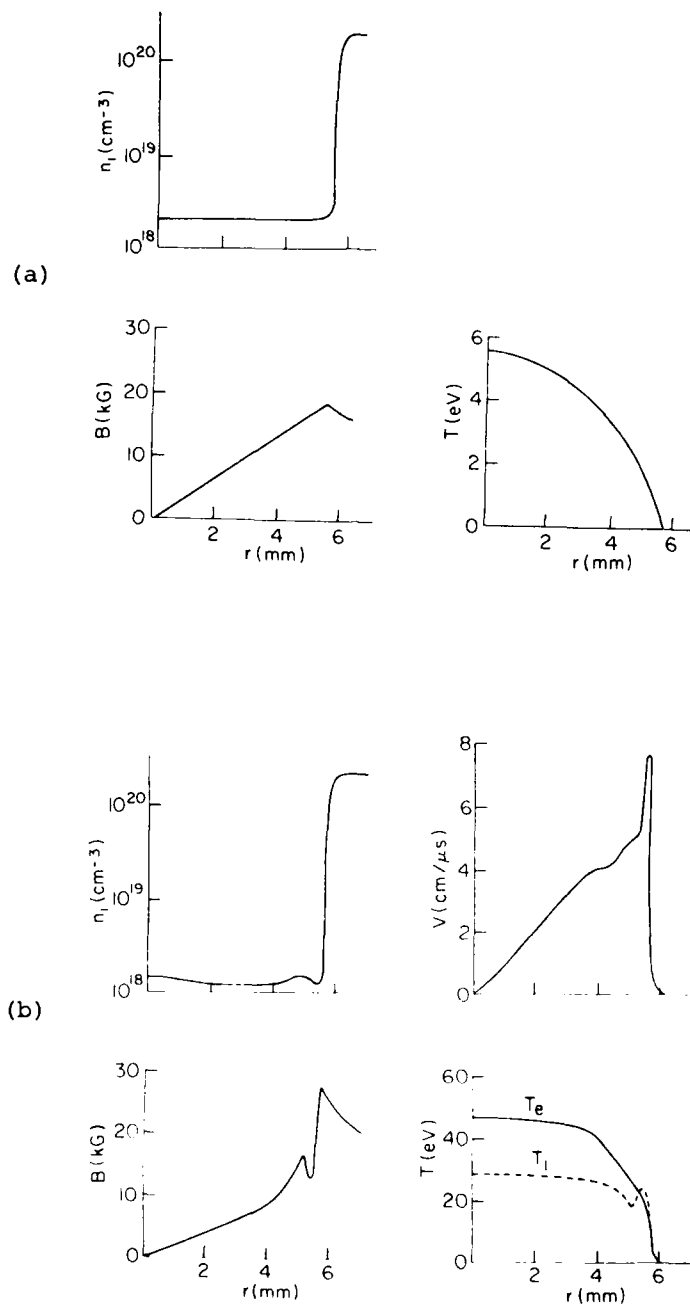
Fig. 18. Initial (a) and final (b) radial profiles in time for
background plasma density, azimuthal magnetic field,
electron and ion temperature ($T_i = T_e$ initially),
and radial plasma velocity ($V=0$ initially).

in amperes and the terms of the right-hand-side are in cgs units. This condition is in qualitative agreement with the results of the MHD code. Because of the greater primary beam deposition, lower-voltage ion beams require lower background density. Thus, the maximum allowed value of $I_b I_{ch}$ is reduced with lower ion voltage. This indicates that less power can be transported in channels carrying lower-voltage ions unless the channel current can be significantly reduced. However, the channel current is determined primarily by the spread of injection angles and θ_M is unlikely to be reduced for less-stiff lower-energy ions. Additionally, Eq. (4) is easier to satisfy with the beam in the bunched state since $I_b \tau$ remains constant as τ is reduced. If a final focusing stage after transport can be employed[26], then the beam can be transported with a radius larger than the pellet size. In this case the constraints of Eq. (4) can be considerably relaxed because of the strong R^4 dependence.

A second important consideration for beam transport channels is the total energy loss suffered by the beam during transport. The energy loss consists of both that due to primary deposition and that due to slowing in the electric field produced by return currents and plasma expansion. For the example considered in Fig. 18, the 5 MV protons lose about 200 kV/m. This energy loss could be reduced or possibly turned into an energy gain[24] if the channel plasma during beam injection is imploding with a velocity of $\sim 10^7$ cm/sec using a 100 kA channel current.

9. BEAM BUNCHING DURING TRANSPORT

Since the time of flight of the ions through the channel to the pellet usually exceeds the beam pulse duration, applying an accelerating voltage ramp at the diode can result in power multiplication (PM) by beam bunching[27]. Since the pulsed-power technology employed results in ion emission times of 50-100 ns and the desired irradiation time on the pellet is about 20 ns, as much as a factor-of-5 bunching is desirable. For purely axial motion, ions accelerated by the ideal voltage waveform

$$\Phi(t) = \frac{\Phi_O}{(1-t/t_a)^2} \; ; \; 0 \leq t \leq \tau < t_a \tag{5}$$

all arrive at the target at the same time t_a. In reality, errors in voltage shape, $\delta\Phi$, and the spread in ion injection angles contribute to a spread in arrival times, δt_a, thus limiting the degree of power multiplication to a factor $\tau/\delta t_a$. For a desired PM factor of 5, analysis indicates that $\delta\Phi/\Phi \lesssim 0.15$ and $\theta_M \lesssim 0.3$ radians are sufficient for parameters of interest.

23
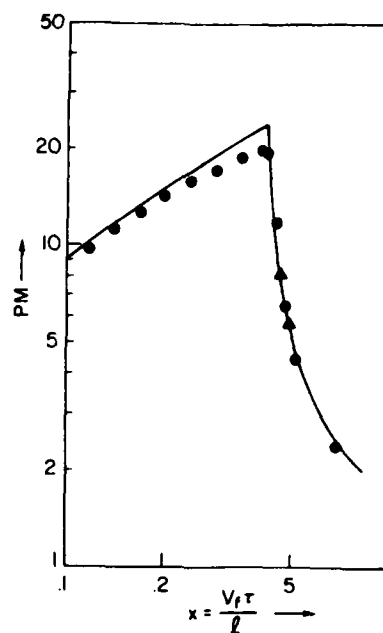
Fig. 19. Theoretically achievable power multiplication predicted
by analytic modeling (solid curve) and macroparticle code.
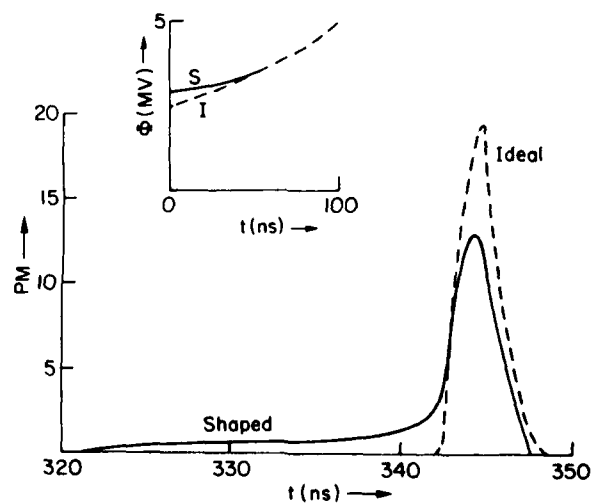
Fig. 20. Bunched pulse shaping.

Figure 19 compares analytic modeling of achievable power multiplication with a macroparticle code, where ℓ is the distance to the target and V_f is the ion speed at $t = \tau$. Below $x = 0.414$, PM is limited by the spread in injection angles $\theta_M = 0.2$ radians. Above this value, PM is determined by a maximum voltage ramp $\Phi_f/\Phi_o = 2$ in order to control the energy spectrum of ions depositing in the pellet.

Figure 20 compares the time variation of power on target using two voltage waveforms and the parameter set $r_s = 0.4$, $R = 0.6$ cm, $\ell = 7.5$ m, $\theta_M = 0.2$ radians. Peak power multiplication is achieved by employing the ideal voltage. In that case, the power multiplication is limited by the dispersion in injection angles. When the accelerating voltage is higher than the ideal early in time, some ions arrive early on target. This results in a shaped foot which may be desirable for some inertial-confinement-fusion target configurations.

10. SYSTEM REQUIREMENTS FOR INERTIAL CONFINEMENT FUSION

Pulsed power, ion focusing, transport, bunching and beam-target interaction considerations can be combined in order to determine an acceptable set of system parameters for the ignition of a high-gain fusion pellet. High voltage beams are easily focused because of their relative insensitivity to time-varying magnetic fields in the diode. However, their long range in materials leads to inefficient energy coupling to fusion targets. Low voltage beams suffer from excessive energy loss in the transport channel and difficulty in focusing. For any voltage, channel hydrodynamic response calculations indicate difficulty in transporting ion beams much in excess of 1 MA without employing a final focusing stage. Thus, for a fixed power and energy requirement delivered to the target, MHD considerations establish a lower limit on the number of channels which can be used to transport ion beams to the target. An upper limit on the number of channels which can be used is set by considerations that include channel creation energy and beam overlap problems. These points are considered in Fig. 21 which defines an acceptable parameter range for a 2 MJ ion beam incident on a high-gain pellet. The SANDIA PBFA concept has design objectives in the lower right-hand corner of the window. Research at NRL concentrates primarily on parameters of the upper left. Table 1 summarizes an acceptable range of system parameters based on the considerations discussed above. Parameters based on two pellet requirements and two ion pulse durations are shown. The stored energy is an estimate of the total electrical energy stored in the Marx generators required to provide the total ion beam energy. The shorter-duration beams require higher powers in the diode but also require less bunching in order to achieve power on target. The focused power represents the total focused ion beam power for all the modules into the entrance of all the channels.
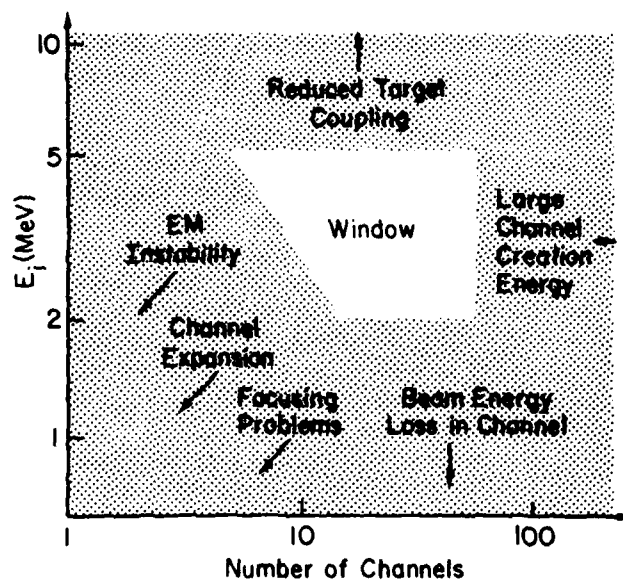
Fig. 21. Channel number considerations for protons in hydrogen.

Table I. Ignition System Parameter.

ENERGY ON PELLET (MJ)	3		2
POWER ON PELLET (TW)	200		100
STORED ENERGY (MJ)	24		16

	24		16	
PULSE DURATION (ns)	100	50	100	50
FOCUSED POWER (TW)	35	70	23	45
POWER MULTIPLICATION	6	3	4.5	2
FOCUSED CURRENT (MA)				
5 MeV PEAK	7	14	4.5	9
2 MeV PEAK	18	35	12	23
MIN. BUNCHING LENGTH (m)				
5 MeV PROTONS	6	2.5	6	2
2 MeV DEUTERONS	3	1	2.5	0.8

Focused current represents the total current transported by all
channels. Using 1 MA as the current which can be transported in any
given channel, the focused current numbers represent an estimate
of the minimum number of channels required to transport the total
beam. The minimum channel length (i.e. stand-off distance) is
arrived at by determining the smallest transport length which can
achieve the desired degree of power multiplication (PM) using an
accelerating voltage which varies by no more than a factor of 2.
This bunching length may be estimated from[21]

$$\frac{V_f \tau}{\ell} = \frac{0.414}{1-1/PM} \; .$$

The scaling of ℓ with PM results from the fact that smaller lengths
than necessary for optimal bunching are sufficient for moderate
power multiplication factors.

Extension of these results to ion species other than $Z = 1$
requires further investigation of transport properties. Higher
voltage beams can transport at lower beam current to achieve beam
powers comparable to $Z = 1$. Channel currents are uncertain. From
Eq. (1), I_{ch} is proportional to the larger values of m/q. However,
it tends to be reduced by the smaller values of θ_M permitted by
better focusing control.

In the near future scaling of present results will be attempted
in the following areas. Diode behavior at the 3-5 TW level on
PITHON will be studied in order to check ion beam efficiency and
focusability. The physics of higher voltage (up to 10 MV) diodes
operating at impedances up to 20 ohms will be studied on the
Harry Diamond Laboratory Aurora generator.[28] Transport of ion
beams will be performed in longer channels where beam bunching may
be investigated. Larger diameter channels with a final focusing
stage will be studied in order to achieve transport of higher
current, longer duration ion beams. The effect of imploding plasma
discharges on the energy of the transported ion beam will be
investigated. These experiments will provide the MA/cm^2 level
fluxes required for relevant ICF beam target studies.

REFERENCES

1. Shyke A. Goldstein and R. Lee, Phys. Rev. Lett. $\underline{35}$, 1079 (1975).
2. J. W. Poukey, J. R. Freeman, M. J. Clauser, and G. Yonas, Phys. Rev. Lett. $\underline{35}$, 1806 (1975).
3. J. W. Poukey, J. Vac. Sci. Technol. $\underline{12}$, 1214 (1975).
4. A. E. Blaugrund, G. Cooperstein, J. R. Boller and Shyke A. Goldstein, Bull. Am. Phys. Soc. $\underline{20}$, 1252 (1975).
5. P. A. Miller, C. W. Mendel, D. W. Swain, and S. A. Goldstein, in Proceedings of the International Topical Conference on Electron Beam Research and Technology, Albuquerque, New Mexico (1975), p. 619; G. Cooperstein, S. J. Stephanakis, J. R. Boller R. Lee, and Shyke A. Goldstein, in Proceedings of the 1976 IEEE International Conference on Plasma Science, Austin, Texas (1976), (IEEE Cat. 76CH1083-5-NPS), p. 126.
6. Shyke A. Goldstein, D. P. Bacon, D. Mosher and G. Cooperstein, Proceedings of the Second International Topical Conference on High Power Electron and Ion Beam Research and Technology, Ithaca, New York (1977) p. 71.
7. D. J. Johnson, G. W. Kuswa, A. V. Farnsworth, Jr., J. P. Quintenz, R. J. Leeper, E. J. T. Burns, and S. Humphries, Jr., Phys. Rev. Lett. $\underline{42}$, 610 (1979); D. J. Johnson, Bull. Am. Phys. Soc. $\underline{24}$, 925 (1979).
8. G. Cooperstein, Shyke A. Goldstein, D. Mosher, F. W. Oliphant, F. L. Sandel, S. J. Stephanakis and F. C. Young in Proceedings 3rd International Topical Conference on High Power Electron and Ion Beam Research and Technology, Novosibirsk, USSR (1979).
9. R. O. Bangerter and D. J. Meeker, in Proceedings of the Second International Topical Conference on High Power Electron and Ion Beam Research and Technology, Ithaca, New York (1977), p.183; J. H. Nuckolls, in Proceedings of the Topical Meeting on Inertial Confinement Fusion, San Diego, CA (1978), (Optical Society of America 78CH1310-2QEA).
10. G. Yonas, Sci. Am. $\underline{239}$, No. 5, 50 (1978); P. A. Miller, D. J. Johnson, T. P. Wright and G. W. Kuswa, Comments on Plasma Physics and Controlled Fusion, $\underline{5}$, 95 (1979).
11. S. J. Stephanakis, J. R. Boller, G. Cooperstein, Shyke A. Goldstein, D. D. Hinshelwood, D. Mosher, W. F. Oliphant, F. C. Young, R. D. Genuario and J. E. Maenchen, Bull. Am. Phys. Soc. $\underline{24}$, 1031 (1979).
12. A. E. Blaugrund, G. Cooperstein, and Shyke A. Goldstein, Phys. Fluids $\underline{20}$, 1185 (1977).
13. J. W. Poukey, in Proceedings of the International Topical Conference on Electron Beam Research and Technology, Albuquerque, New Mexico (1975), p. 247.
14. S. J. Stephanakis, D. Mosher, G. Cooperstein, J. R. Boller, J. Golden, and Shyke A. Goldstein, Phys. Rev. Lett. $\underline{37}$, 1543 (1976).
15. Shyke A. Goldstein, G. Cooperstein, Roswell Lee, D. Mosher and S. J. Stephanakis, Phys. Rev. Lett. 40, 1504 (1978).

16. J. R. Boller, J. K. Burton, and J. D. Shipman, Jr., in Proceedings of the IEEE Second International Pulsed Power Conference, Lubbock, Texas (1979).

17. F. C. Young, J. Golden, and C. A. Kapetanakos, Rev. Sci. Instrum. 48, 432 (1977).

18. Shyke A. Goldstein, A. T. Drobot in Proceedings of 1979 IEEE International Conference on Plasma Science, Quebec (1979), (IEEE Cat. 79CH1410-ONPS), p. 161.

19. R. Lee and Shyke A. Goldstein, NRL Memorandum Report 3702 (1978); D. Mosher, G. Cooperstein and Shyke A. Goldstein, NRL Memorandum Report 4130 (1979).

20. A. T. Drobot, R. J. Barker, R. Lee, A. Sternlieb, D. Mosher and Shyke A. Goldstein, in Proceedings 3rd International Topical Conference on High Power Electron and Ion Beam Research and Technology, Novosibirsk, USSR (1979).

21. P. F. Ottinger, D. Mosher, Shyke A. Goldstein, in Proceedings 1979 IEEE International Conference on Plasma Science, Quebec (1979), (IEEE Cat. 79CH1410-ONPS), p. 105.

22. P. F. Ottinger, D. Mosher and Shyke A. Goldstein, Phys. Fluids 22, 332 (1979); P. F. Ottinger, D. Mosher and Shyke A. Goldstein to be published in Phys. Fluids (1980).

23. J. Golden, R. A. Mahaffey, J. A. Pasour, F. C. Young, C. A. Kapetanakos, Rev. Sci. Instrum. 49, 1384 (1978).

24. Shyke A. Goldstein and D. A. Tidman, private communication.

25. D. G. Colombant, Shyke A. Goldstein, D. Mosher, in Proceedings 1979 IEEE International Conference on Plasma Science, Quebec (1979), (IEEE Cat. 79CH1410-ONPS), p. 105.

26. P. F. Ottinger, Shyke A. Goldstein and D. Mosher, private communication.

27. D. Mosher, Shyke A. Goldstein, Bull. Am. Phys. Soc. 23, 800 (1978).

28. B. Bernstein, I. Smith, IEEE Trans. Nucl. Sci. 20, 294 (1973).

DISTRIBUTION LIST

Director
Defense Intelligence Agency
Washington, DC 20301

Attn: DTICI Robert I. Rubenstein   1 copy

Defense Advanced Research Project Agency
1400 Wilson Blvd.
Arlington, VA 22209
Attn: R. Bayless   1 copy

Director
Defense Nuclear Agency
Washington, DC 20305

Attn: FCPR   1 copy
      STVL   1 copy
      TISI Archives   1 copy
      TITL Tech. Library   3 copies
      J. Z. Farber (RAEV)   1 copy
      R. L. Gullickson (RAEV)   1 copy

Defense Technical Information Center
Cameron Station
5010 Duke Street
Alexandria, VA 22314

Attn: T. C.   12 copies

Under Sec'y of Defense for RSCH and ENGRG
Department of Defense
Washington, DC 20301

Attn: S&SS(OS)   1 copy

Chief
Livermore Division Fld Command DNA
Lawrence National Laboratory
P. O. Box 808
Livermore, CA 94550

Attn: FCPRL   1 copy

National Technical Information Service
U.S. Department of Commerce
5285 Port Royal Road
Springfield, VA 22161   24 copies

Commander
BMD System Command
P. O. Box 1500
Huntsville, AL 35807

Attn: SSC-TEN   1 copy

DEP Chief of Staff for RSCH DEV & ACQ
Department of the Army
Washington, DC 20310

Attn: DAMA-CSM-N   1 copy

Commander
Harry Diamond Laboratories
2800 Powder Mill Road
Adelphi, MD 20783
(CNWDI-INNER ENVELOPE: ATTN: DELHD-RBH)

Attn: DELHD-NP   1 copy
      DELHD-RCC J. A. Rosado   1 copy
      DRXDO-RBH P. A. Caldwell   1 copy
      DRXDO-RBH D. Schallhorn   1 copy
      DRXDO-TI   Tech Lib.   1 copy
      S. Graybill   1 copy

Commander
Picatinny Arsenal
Dover, NJ 07801

Attn: SMUPA ND-N-E   1 copy

Commander
U. S. Army Missile Command
Redstone Arsenal, AK 35809

Attn: Redstone Scientific Information CTR
      DRCPM-PM-PE-EA   1 copy

Commander
U. S. Army Nuclear Agency
7500 Backlick Road
Building 2073
Springfield, VA 22150

Attn: ATCN-W   1 copy

Commander
U. S. Army Test and Evaluation COMD
Aberdeen Proving Ground, MD 21005

Attn: DRSTE-EL   1 copy

Commander
Naval Electronic Systems CMD HQS
Washington, DC 20360

Attn: Code 5032   1 copy

Commanding Officer
Naval Intelligence Support Center
4301 Suitland Road - Building 5
Washington, DC 20390

Attn: NISC-45   1 copy

31

Naval Research Laboratory
  Addressee: Attn: Name/Code
  Code 2628 - TIC-Distribution   25 copies
  Code 4020 - J. Boris   1 copy
  Code 6682 - D. Nagel   1 copy
  Code 4700 - T. Coffey   25 copies
  Code 4707 - J. Davis   1 copy
  Code 4730 - S. Bodner   1 copy
  Code 4740 - V. Granatstein   1 copy
  Code 4760 - B. Robson   1 copy
  Code 4761 - C. Kapetanakos   1 copy
  Code 4770 - Branch Head   10 copies
  Code 4770.1 I. Vitkovitsky   1 copy
  Code 4771 - D. Mosher   10 copies
  Code 4773 - G. Cooperstein   10 copies
  Code 4790 - D. Colombant   1 copy
  Code 4790 - I. Haber   1 copy
  Code 4790 - M. Lampe   1 copy

Officer-in-Charge
Naval Surface Weapons Center
White Oak, Silver Spring, MD 20910

Attn: Code WR43   1 copy
       Code WA501 - Navy Nuc Prgms Off   1 copy

Chief of Naval Operations
Navy Department
Washington, DC 20350

Attn: R. A. Blaise 604C4   1 copy

Commander
Naval Weapons Center
China Lake, CA 93555

Attn: Code 533 Tech Lib.   1 copy

AF Weapons Laboratory, AFSC
Kirtland AFB, NM 87117

Attn: CA   1 copy
       ELC   1 copy
       NT   1 copy
       SUL   1 copy
       DYP   1 copy
       J. Darrah   1 copy
       W.L. Baker   1 copy

HQ USAF/RD
Washington, DC 20330

Attn: RDQSM   1 copy

Director
Joint Strat TGT Planning Staff JCS
OFFUTT AFB
Omaha, NB 68113

Attn: JSAS   1 copy

SAMSO/DY
Post Office Box 92960
Worldway Postal Center
Los Angeles, CA 90009
(Technology)

Attn: DYS   1 copy

SAMSO/IN
Post Office Box 92960
Worldway Postal Center
Los Angeles, CA 90009

Attn: IND MAJ D. S. Muskin   1 copy

SAMSO/MN
Norton AFB, CA 92409
(Minuteman)

Attn: MNNH   1 copy

SAMSO/SK
Post Office Box 92960
Worldway Postal Center
Los Angeles, CA 90009
(Space Comm Systems)

Attn: SKF P. H. Stadler   1 copy

U. S. Department of Energy
Division of Inertial Fusion
Washington, DC 20545

Attn: G. Canavan   2 copies
       T. F. Godlove   1 copy
       S. L. Kahalas   1 copy

Argonne National Laboratory
9700 South Cass Avenue
Argonne, Illinois 60439

Attn: G. R. Magelssen   1 copy
       R. J. Martin   1 copy

Brookhaven National Laboratory
Upton, NY 11973

Attn: A. F. Maschke   1 copy

Lawrence Berkley Laboratory
Berkeley, CA 94720

Attn: D. Keefe   1 copy

Lawrence Livermore National Laboratory
P. O. Box 808
Livermore, CA 94550

Attn: L-18	1 copy
L-153	1 copy
R. O. Bangerter	1 copy
R. J. Briggs	1 copy
E. P. Lee	1 copy
J. H. Nuckolls	1 copy
S. S. Yu	1 copy
Tech Info Dept. L-3	1 copy

Los Alamos National Laboratory
P. O. Box 1663
Los Alamos, NM 87545

Attn: D. B. Henderson	1 copy
R. B. Perkins	1 copy
L. E. Thode	1 copy

National Bureau of Standards
Washington, DC 20234

Attn: J. Leiss	1 copy

National Science Foundation
Mail Stop 19
Washington, DC 20550

Attn: O. Berley	1 copy

Sandia National Laboratories
P. O. Box 5800
Albuquerque, NM 87115

Attn: J. P. Freeman	1 copy
S. Humphries	1 copy
D. J. Johnson	1 copy
G. W. Kuswa	1 copy
P. S. Miller	1 copy
J. P. Vandevender	1 copy
G. Yonas	1 copy
Doc Con for 3141 Sandia RPT Coll	1 copy

AVCO Research and Systems Group
201 Lowell Street
Wilmington, MA 01887

Attn: Research Lib. A830 Rm. 7201	1 copy

BDM Corporation, The
7915 Jones Branch Drive
McLean, VA 22101

Attn: Tech Lib.	1 copy

Boeing Company, The
P. O. Box 3707
Seattle, WA 98124

Attn: Aerospace Library	1 copy

Cornell University
Ithaca, NY 14850

Attn: D. A. Hammer	1 copy
R. N. Sudan	1 copy
J. Maenchen	1 copy

Dikewood Industries, Inc.
1009 Bradbury Drive, SE
Albuquerque, NM 87106

Attn: L. W. Davis	1 copy

EG&G, Inc.
Albuquerque Division
P. O. Box 10218
Albuquerque, NM 87114

Attn: Technical Library	1 copy

Ford Aerospace & Communications Operations
Ford & Jamboree Roads
Newport Beach, CA 92663
(Formerly Aeronutronic Ford Corporation)

Attn: Tech Info Section	1 copy

Ford Aerospace & Communications Corp
3939 Fabian Way
Palo Alto, CA 94303
(Formerly Aeronutronic Ford Corporation)

Attn: Library	1 copy
D. R. McMorrow MS G 30	1 copy

General Electric Company
Space Division
Valley Forge Space Center
Goddard Blvd., King of Prussia
P. O. Box 8555
Philadelphia, PA 19101

Attn: J. C. Peden VFSC, Rm. 4230M	1 copy

General Electric Company
Tempo-Center for Advanced Studies
816 State Street (P. O. Drawer QQ)
Santa Barbara, CA 93102

Attn: DASIAC	1 copy

Grumman Aerospace Corporation
Bethpage, NY 11714

Attn: P. Suh	1 copy

Institute for Defense Analyses
400 Army-Navy Drive
Arlington, VA 22202

Attn: IDA Librarian R. S. Smith	1 copy

33

Ion Physics Corporation
South Beford Street
Burlington, MA 01803

Attn: H. Milde   1 copy

Ian Smith Associates
3115 Gibbens Dr.
Alameda, CA 94501
Attn: I. Smith   2 copies

IRT Corporation
P. O. Box 81087
San Diego, CA 92138

Attn: R. L. Mertz   1 copy

JAYCOR, Inc.
205 S. Whiting Street
Alexandria, VA 22304

Attn: J. Guillory   1 copy
      R. Hubbard   1 copy
      R. Sullivan   1 copy
      D. A. Tidman   1 copy

JAYCOR, Inc.
1401 Camino Del Mar
Del Mar, CA 92014

Attn: E. Wenaas   1 copy

JAYCOR, Inc.
300 Unicorn Park Drive
Woburn, MA 01801

Attn: H. Linnerud   1 copy

Kaman Science Corporation
P. O. Box 7463
Colorado Springs, CO 80933

Attn: A. P. Bridges   1 copy
      D. H. Bryce   1 copy
      J. R. Hoffman   1 copy
      W. E. Ware   1 copy

Lockheed Missiles and Space Co., Inc.
3251 Hanover Street
Palo Alto, CA 94304

Attn: L. F. Chase   1 copy

MIT
Massachusetts Institute of Technology
Cambridge, MA 02139

Attn: R.C. Davidson   1 copy
      G. Bekefi   1 copy
      D. Hinshelwood   1 copy

Maxwell Laboratories, Inc.
9244 Balboa Avenue
San Diego, CA 92123

Attn: R. W. Clark   1 copy
      A. C. Kolb   1 copy
      P. Korn   1 copy
      A. R. Miller   1 copy
      J. Pearlman   1 copy

McDonnell Douglas Corporation
5301 Bolsa Avenue
Huntington Beach, CA 92647

Attn: S. Schneider   1 copy

Mission Research Corporation
1400 San Mateo Blvd. SE
Albuquerque, NM 87108

Attn: B. B. Godfrey   1 copy

Mission Research Corporation-San Diego
P. O. Box 1209
LaJolla, CA 92038

Attn: V.A.J. Van Lint   1 copy

Mission Research Corporation
735 State Street
Santa Barbara, CA 93101

Attn: W. C. Hart   1 copy
      C. L. Longmire   1 copy

Northrop Corporation
Electronic Division
2301 West 120th Street
Hawthorne, CA 90250

Attn: V. R. DeMartino   1 copy

Northrop Corporation
Northrop Research and Technology Ctr.
3401 West Broadway
Hawthorne, CA 90205   1 copy

Physics International Co.
2700 Merced Street
San Leandro, CA 94577

Attn: J. Benford   1 copy
      B. Bernstein   1 copy
      R. Genuario   1 copy
      E. B. Goldman   1 copy
      A. J. Toepfer   1 copy

Pulsar Associates, Inc.
11491 Sorrento Valley Blvd.
San Deigo, CA 92121

Attn: C. H. Jones, Jr.   1 copy

34

R&D Associates
P. O. Box 9695
Marina Del Rey, CA 90291

University of California
Dept. of Physics
La Jolla, CA 92037

Attn: W. R. Graham, Jr.	1 copy
M. Grover	1 copy
C. MacDonald	1 copy
E. Martinelli	1 copy
L. Schlessinger	1 copy

Attn: K. Brueckner   1 copy

University of California
Boelter Hall 7731
Los Angeles, CA 90024

Science Applications, Inc.
P. O. Box 2351
LaJolla, CA 92038

Attn: F.F. Chen   1 copy

Attn: J. Robert Beyster   1 copy

University of California
Irvine, CA 90024

Attn: G. Benford	1 copy
N. Rostoker	1 copy

Spire Corporation
P. O. Box 0
Bedford, MA 01730

University of Illinois
Urbana, IL 61801

Attn: R. G. Little   1 copy

Attn: G. H. Miley	1 copy
J. T. Verdeyen	1 copy

SRI International
333 Ravenswood Avenue
Menlo Park, CA 94025

University of Rochester
Laboratory of Laser Energetics
River Station, Hopeman 110
Rochester, NY 14627

Attn: Setsuo Odairiki   1 copy

Stanford University
SLAC
P. O. Box 4349
Stanford, CA 94305

Attn: M. J. Lubin   1 copy

U. S. Department of Energy
P. O. Box 62
Oak Ridge, TN 37830   50 copies

Attn: W. B. Herrmannsfeldt   1 copy

Systems, Science and Software, Inc.
P. O. Box 4803
Hayward, CA 94540

Vought Corporation
Michigan Division
38111 Van Dyke Road
Sterling Heights, MI 48077
(Formerly LTV Aerospace Corp)

Attn: D. A. Meskan   1 copy

Systems, Science and Software, Inc.
P. O. Box 1620
LaJolla, CA 92038

Attn: Tech Lib   1 copy

Attn: A. R. Wilson   1 copy

Bhabha Atomic Research Centre
Bombay - 400085, India

Attn: B. K. Godwal   1 copy

Texas Tech University
P. O. Box 5404 North College Station
Lubbock, TX 79417

CEA, Centre de Etudes de Lemeil
B. P. 27
94190 Villeneuve, Saint George
France

Attn: T. L. Simpson   1 copy

TRW Defense and Space Sys Group
One Space Park
Redondo Beach, CA 90278

Attn: A. Bernard	1 copy
A. Jolas	1 copy

Attn: Tech Info Center/S-1930   1 copy

CEA, Centre de Etudes de Valduc
P. B. 14
21120 Is-sur-Tille
France

Attn: J. Barbaro	1 copy
C. Bruno	1 copy
N. Camarcat	1 copy
C. Patou	1 copy
C. Peugnet	1 copy

Centro Di Frascati
C.P.N. 65
00044 Frascati (Roma)
Italy

Attn: J.P. Rajer   1 copy

Ecole Polytechnique
Labo. PMI
91128 Palaseau Cedex
France

Attn: J. M. Buzzi   1 copy
       H. Doucet   1 copy

Institut d'Electronique Fondamentale
Universite' Paris XI-Bat. 220
F91405 Orsay
France

Attn: G. Gautherin   1 copy

Institut Fur Neutronenphysik
   un Reaktortechnik
Postfach 3640
Kernforschungszentrum
D-7500 Karlsruhe 1
West Germany

Attn: H. U. Karow   1 copy
       W. Schmidt   1 copy

Institute of Atomic Energy
Academia Sinica - Peking
People's Republic of China

Attn: R. Hong   1 copy

Institute of Laser Engineering
Osaka University
Yamadakami
Suita
Osaka 565, Japan

Attn: K. Imasaki   1 copy
       S. Nakai   1 copy

Instituto De Investigaciones Cientificas Y Technicas
         De Las Fuerzas Armadas
Aufriategui y Varela
V. Martelli 1603
Pcia Bs. As. - R. Argentina

Attn: N. B. Camusso   1 copy

Max-Planck-Institut fur Plasmaphysik
8046 Garching bei Munchen
West Germany

Attn: R. Lengyel   1 copy

Physical Research Laboratory
Navrangpura
Ahmedabad - 380009 - India

Attn: V. Ramani   1 copy

Shivaji University
Kolhapur, India

Attn: L. N. Katkan   1 copy

Weizmann Institute of Science
Rehovot, Israel

Attn: A. E. Blaugrund   1 copy
       E. Nardi   1 copy
       Z. Zinamon   1 copy

DATE:
FILME